npj | computational materials

Article

Published in partnership with the Shanghai Institute of Ceramics of the Chinese Academy of Sciences

https://doi.org/10.1038/s41524-025-01747-7

Machine-learning-accelerated mechanistic exploration of interface modification in lithium metal anode

Genming Lai[1,4], Ruiqi Zhang[1,4], Chi Fang[1], Juntao Zhao[1], Taowen Chen[2], Yunxing Zuo[2] ✉, Bo Xu[3] ✉ & Jiaxin Zheng[1] ✉

Although the electrode-electrolyte interface is a crucial electrochemical region, the comprehensive understanding of interface reactions is limited by the time and space scales of experimental tools. Theoretical simulations with this delicate interface also remain one of the most significant challenges for atomistic modeling, particularly for the stable long-timescale simulation of the interface. Here we introduce a novel scheme, hybrid ab initio molecular dynamics combined with machine learning potential (HAML), to accelerate the modeling of electrode-electrolyte interface reactions. We demonstrate its effectiveness in modeling the interfaces of Li metal with both liquid and solid-state electrolytes, capturing critical processes over extended time scales. Furthermore, we reveal the role of interface reaction kinetics in interface regulation through HAML simulations, combined with the similarity analysis method. It is demonstrated that element (Se, F, O) doping in the Li_6PS_5Cl system is an effective strategy for enhancing interface reaction kinetics, facilitating the formation of a more stable interface protective layer faster at room temperature. Moreover, moderate structural instability can positively contribute to interface stabilization. HAML offers a promising approach for addressing the challenge of designing stable interfaces while reducing computational costs. This work provides valuable insights for advancing the understanding and optimization of interface behaviors in Li metal batteries.

The electrode-electrolyte interface is a critical region where various physical and chemical processes occur, encompassing activities from energy conversion and storage to electrochemistry[1–3]. Li metal is widely regarded as an ideal anode material for next-generation secondary batteries due to its extremely low electrochemical potential (−3.04 V vs. the standard hydrogen electrode) and ultrahigh theoretical capacity (3860 mAh g^{-1})[4–7]. However, the commercial application of the Li metal anode remains challenging due to several key issues, including uncontrollable Li dendrite growth, irreversible interface reactions, and mechanical instability of solid-electrolyte interphase (SEI)[7,8]. These issues are closely tied to the interface between the Li metal anode and liquid or solid-state electrolytes. The complexity of these challenges stems from the dynamic nature of the interface, which is further complicated by the nanoscale dimensions of the involved reactions, as well as the complex physicochemical interactions that occur. For instance, element doping is commonly used to improve the lithium-ion conductivity of solid-state electrolytes (SSEs). Furthermore, element doping has also been shown to modify the interface properties such as the stability of the Li|SSE interface, which in turn affects the overall cycling performance of the battery[9,10]. However, the universal principles governing the dynamic evolution of the interface after element doping remain unclear.

Experimental characterizations of the interface reactions remain challenging due to their nanoscale dimensions, dynamic nature, and the interplay of multiple physicochemical processes[11,12]. Theoretical simulations have emerged as indispensable tools for investigating the mechanisms governing interface reactions, potentially serving as realistic in situ characterization techniques[11,13,14]. Therefore, efficiently modeling these complex interface reactions is crucial for the development of a safe and stable Li metal anode. There are several approaches to model interface reactions on the Li metal anode. Ab initio molecular dynamics (AIMD) simulations, known for accurately describing atomic interactions, have been utilized to explore the microscopic intricacies of the interface between Li metal and electrolyte[15–18]. Nevertheless, the accessible space and time scales of simulations are

---

[1] School of Advanced Materials, Peking University, Shenzhen Graduate School, Shenzhen, People's Republic of China. [2] EACOMP, Shenzhen, People's Republic of China. [3] GAC Aion New Energy Automobile Co., Ltd., Guangzhou, People's Republic of China. [4] These authors contributed equally: Genming Lai, Ruiqi Zhang.
✉ e-mail: zuoyunxing@eacomp.com; xubo@aion.com.cn; zhengjx@pkusz.edu.cn

constrained by the high computational cost[19]. Conversely, molecular dynamics (MD) simulations serve as an ideal tool for investigating dynamic processes at a higher speed. However, MD simulations are often hindered by the limited availability and accuracy of classical force fields, which rely on physical approximations[20,21]. In recent years, artificial intelligence technologies have become increasingly mature[22]. As an effective tool, machine learning potential (MLP) has significantly enhanced the atomic-scale understanding of mechanisms behind many physical phenomena[20,23,24]. The MLP method has demonstrated its potential as a promising alternative, combining speed and accuracy. It has been implemented in battery systems, such as Li metal systems[25,26], solid-state electrolytes,[27,28] and liquid electrolytes[29]. However, the challenges still remain in sampling the vast configuration space and ensuring that MLP is trained on a sufficiently diverse dataset to maintain its reliability in complex simulations, such as distribution shift, particularly for the electrode-electrolyte interface reactions[30–33].

The active learning (AL) strategy has been proposed as an effective sampling method, significantly advancing the development of MLP, through approaches such as on-the-fly AL[34], uncertainty-driven dynamics,[35] and hyperactive learning[36]. However, its application to interface reactions presents several challenges[31,32]. Interface reactions require the simultaneous exploration of the chemical diversity and non-equilibrium thermodynamic pathways, such as reaction intermediates and ion migration[3,37]. However, AL strategies often prioritize the exploration of high-energy or high-variance regions, which do not necessarily align with the actual reaction pathway, thereby introducing sampling bias[38,39]. Additionally, during interface reactions, the continuous evolution of atomic configurations shifts the distribution of training data away from the actual reaction pathway[40,41]. Although adequate sampling can partially alleviate this problem, it struggles to adapt to the abrupt structural changes in non-equilibrium processes and leads to increased computational costs. The key contradiction lies in the conflict between AL's strategy of exploring unknown atomic structures and the need to focus on key reaction pathways in interface reactions, leading to inefficient sampling[41]. On the other hand, electrode-electrolyte interfaces involve multi-element doping, solvation effects, and charge transfer, resulting in a highly complex configuration space[3]. The sampling density of AL often falls short of requirements and does not sufficiently cover enough high-energy transition states or extreme configurations, leading to incomplete local fitting of the potential energy surface. This may lead to instability in simulations and ultimately cause simulation collapse[40–42]. Addressing these challenges requires refining AL strategies to focus on targeted sampling aligned with interface reaction mechanisms and critical configurations.

Herein, we introduce a hybrid framework that combines AIMD and MLP to model the electrode-electrolyte interface. The innovation of HAML lies in its ability to guide reaction pathways in situ, with the coupled AIMD steering the MLP toward physically relevant configurations. This architecture enables HAML to achieve stable long-timescale simulations of interface reactions, addressing the distribution shift challenge in MLP when dealing with complex interface configurations. HAML significantly enhances efficiency and streamlines the simulation process. We applied the method to model interface reactions between Li metal and both liquid electrolytes and solid-state electrolytes, demonstrating its high accuracy and efficiency in capturing key reaction processes and products over extended time scales. Furthermore, we highlight the role of element doping in modifying the interface properties and improving the cycling stability of the Li metal anode. Similarity analysis was employed to assess the severity of the interface reaction, revealing that the changes in the interface reaction kinetics are the essential reason for interface modification. These efforts will deepen the understanding of the Li metal anode interface and facilitate the design of more stable electrode-electrolyte interfaces for safer Li metal batteries.

Results

Hybrid AIMD-MLP method for addressing challenges in interface modeling

Several challenges exist in modeling electrode-electrolyte interfaces due to the inherent complexity of the system, as illustrated in Fig. 1a, b. The primary challenges arise from distribution shift, inefficient sampling of interface configurations, and direction bias. These may result in unrealistic interface behaviors, ultimately leading to the collapse of MD simulations[42]. To address these challenges, we propose a hybrid approach that combines AIMD with MLP, termed HAML, which is primarily inspired by the architecture of HAIR[43]. The workflow of HAML, as illustrated in Fig. 1c, consists of several steps including geometry optimization, AIMD, MLP training, and MLP-driven molecular dynamics (MLP-MD). The essence of HAML lies in the iterative cycles between AIMD, MLP training, and MLP-MD. In each cycle, the final configuration from AIMD serves as the initial configuration for MLP-MD, while the final configuration from MLP-MD becomes the initial configuration for AIMD. This iterative process continues until the predefined simulation time or number of cycles is reached.

In this method, the purposes of AIMD are to provide training data for subsequent MLP training and enhance the accuracy of critical steps in the reaction process. The role of MLP-MD is to accelerate the reaction process, with its main focus on ensuring the reliability of the MLP-MD simulations. To ensure reliability, we adopt the Maxvol algorithm used in moment tensor potential (MTP)[44,45], which monitors the reliability of MLP predictions during MLP-MD simulations to determine whether the MLP-MD should be interrupted. During MLP-MD, the extrapolation grade, denoted as γ, is computed for each assessed configuration. Configurations well-represented

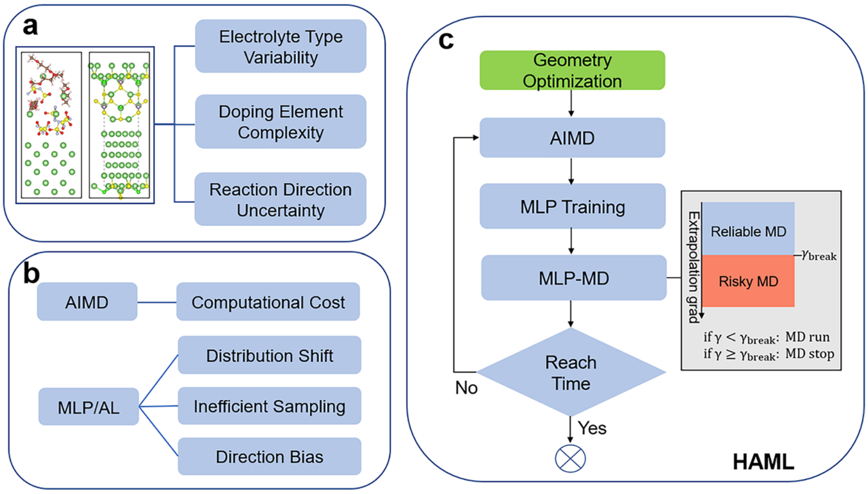

Fig. 1 | Schematic of the HAML method. **a** Schematic illustrating the challenges in understanding the interfaces between Li metal anode and liquid or solid-state electrolytes. **b** Schematic depicting the challenges in modeling these interfaces. **c** Schematic of the HAML, the workflow comprises geometry optimization as well as the iterative cycle of AIMD, MLP training, and MLP-MD.

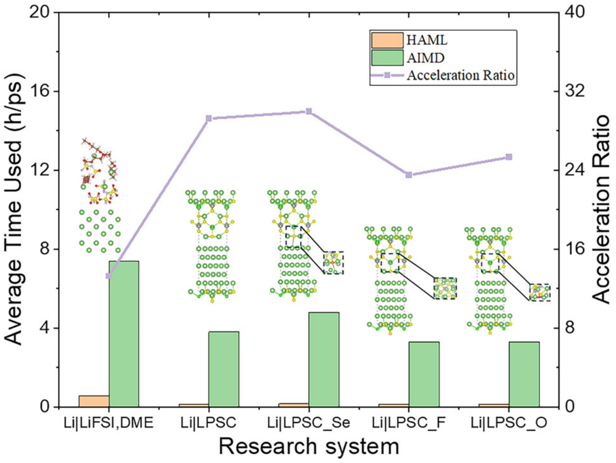

Fig. 2 | Comparison of HAML and AIMD in terms of the average time used and acceleration ratio. The tested systems include interface between Li metal and LiFSI, DME mixed solution (Li|LiFSI,DME), interfaces between Li metal and LPSC system (Li|LPSC), Se-doped system (Li|LPSC_Se), F-doped system (Li|LPSC_F), O-doped system (Li|LPSC_O).

in the training dataset, and thus likely well described by MTP, exhibit a low value of γ. When γ exceeds a predefined threshold γ_{break}, the MLP-MD simulation is interrupted to prevent unreasonable configurations and reactions. This treatment ensures the accuracy and reliability of the HAML approach.

The key innovation of HAML lies in its ability to guide the reaction pathway in situ, with AIMD steering the MLP toward physically relevant configurations. Therefore, HAML offers accuracy similar to that of AIMD while significantly improving efficiency. Compared to pure MLP/AL, HAML eliminates the need for repeated exploration of the configuration space, significantly enhancing efficiency. Moreover, it can conveniently predict the interface evolution through a single simulation. Thus, HAML provides a new opportunity to achieve efficient in situ observation of interface reactions while ensuring high accuracy.

Demonstration of the advancements of the HAML method

In this section, we demonstrate the advantages, accuracy, and efficiency of the HAML through its application to interface reactions between Li metal and both liquid and solid-state electrolytes. The LiFSI, DME mixed solution system, the Li_6PS_5Cl (LPSC) system, and their element-doped systems were selected as research subjects. The initial structures are shown in Supplementary Figs.1 and 2. To highlight the advantages of the HAML method, we compared the computational time required for these simulations. We recorded the total CPU time for HAML and AIMD in each simulation (Supplementary Tables 1–5). For comparison, we further calculated the average time used by HAML and AIMD and plotted the acceleration ratio curve. As shown in Fig. 2, the real-time computational cost relative to the simulation time was reduced to 0.558 h ps^{-1} compared to the AIMD simulation cost of 7.398 h ps^{-1} for the interface between Li metal and LiFSI, DME mixed solution system. For the interfaces between Li metal and LPSC system as well as their element-doped variants (LPSC_Se, LPSC_F, LPSC_O), the real-time computational cost relative to the simulation time was reduced to 0.13~0.16 h ps^{-1} compared to the AIMD simulation cost of 3.29~4.79 h ps^{-1}. The results indicate that HAML achieved a speedup of more than 10 times compared to AIMD for the Li metal and liquid electrolyte system, while for the solid-state electrolyte system, a speedup of over 20 times is achieved. The acceleration performance of HAML simulations in these interfaces demonstrates the generality of the HAML method. Additionally, the temperature stability of AIMD and MLP-MD during HAML simulations shows smooth transitions between the cycles, indicating that the HAML simulations are continuous and smooth (Supplementary Figs. 3–7).

As an example, we demonstrate the application of HAML to model the interface reactions between Li metal and LiFSI, DME mixed solution. We conducted 90 cycles of HAML, extending the reaction time to 420 ps (Fig. 3a), with the NVT canonical ensemble at 300 K. Figure 3b, c presents the trajectory snapshots at 12 ps and 420 ps, respectively. The results show that while some decomposition of the salt occurs at 12 ps, it is incomplete, and many Li atoms at the bottom have not yet participated in the reaction. In contrast, at the extended timescale of 420 ps, the system undergoes a more complete reaction. Combining the radial distribution functions (Fig. 3d–f), the deep reaction products of LiFSI, such as Li_2S and Li_3N, are observed at 420 ps. The complete product statistics and comparison are listed in Supplementary Table 6. These products have been observed in previous experimental studies[46–48]. The results confirm the accuracy and efficiency of HAML. Furthermore, they emphasize the necessity of long-timescale simulations for studying the interface.

These results demonstrate that HAML has the potential to become a comprehensive framework that can achieve stable long-timescale simulations of interface reactions and efficiently predict the interface evolution in various scenarios. This would be essential for optimizing interface properties and the ultimate battery performance in practical applications.

Interface reaction kinetics for promoting interface stability

SSEs have been extensively studied as key components of solid-state Li metal batteries due to their enhanced safety and energy density. Among them, LPSC is a widely used SSE, owing to its high ionic conductivity ($\sim10^{-2}$ S cm^{-1} at room temperature) and cost-effectiveness[49–51]. However, the cycling performance of LPSC in Li metal batteries is limited due to interface side reactions, which can lead to an increase in interfacial resistance and poor electrochemical performance[51–54]. The detailed and accurate micro-mechanism of these interface reactions remains unclear, primarily due to the lack of characterization tools. Consequently, AIMD simulations have been employed to investigate the dynamic reaction mechanism at the interface between Li metal and SSEs[55,56]. However, AIMD simulations are computationally expensive and unsuitable for long-term simulations. To address this limitation, we apply the proposed HAML method to investigate the reactions at the interface between Li metal and LPSC.

We constructed a Li|LPSC interface model consisting of 112 atoms with a mismatch rate of 3.9%. The detailed construction of the model is described in the Supplementary Note 1. Following the HAML simulation at 300 K, completed 528 ps HAML simulation within 20 cycles (Fig. 4a), the Li|LPSC interface underwent significant reactions. As shown in Fig. 4b–d, the structure of the LPSC layer near the Li metal slab exhibited continuous distortion and decomposition, leading to the formation of products. The PS_4^{2-} polyhedron underwent significant breakdown, as evidenced by the disappearance of P–S bonds and the P–S peak at approximately 2 Å after 528 ps (Fig. 4e, f), which aligns with XPS characterization findings that show the instability of P–S bonds[57]. The number of Li–Cl bonds and Li–S bonds is also reduced after 528 ps simulation as a result of the decomposition of LPSC. As shown in Supplementary Fig. 8, the newly formed Li–Cl peak at around 4.5 Å indicates the presence of a Li–Cl interaction in the second coordination sphere, which corresponds to the LiCl product at the interface. Additionally, the increase in Li–P bond number after the reaction corresponds to the formation of Li_3P. The observed final products include Li_3P, Li_2S, and LiCl, consistent with previous computational and experimental studies[55–58]. Furthermore, we extended the simulation time from 528 ps to 1 ns but observed no obvious change in the interface structure (Supplementary Fig. 9). This phenomenon is similar to former computational researches[55,58,59], which indicates the uncomplete reaction between LPSC and Li and the failure in constructing a stable SEI to avoid side reactions, thus make the interface intrinsically unstable when cycling at high rate. In addition, we calculated the ionic conductivity of LPSC (Supplementary Fig. 10), providing quantitative validation for the accuracy of the HAML method.

One of the modification methods to modify the interfacial structure of Li|LPSC is to introduce doping elements. Among the doping elements, Se

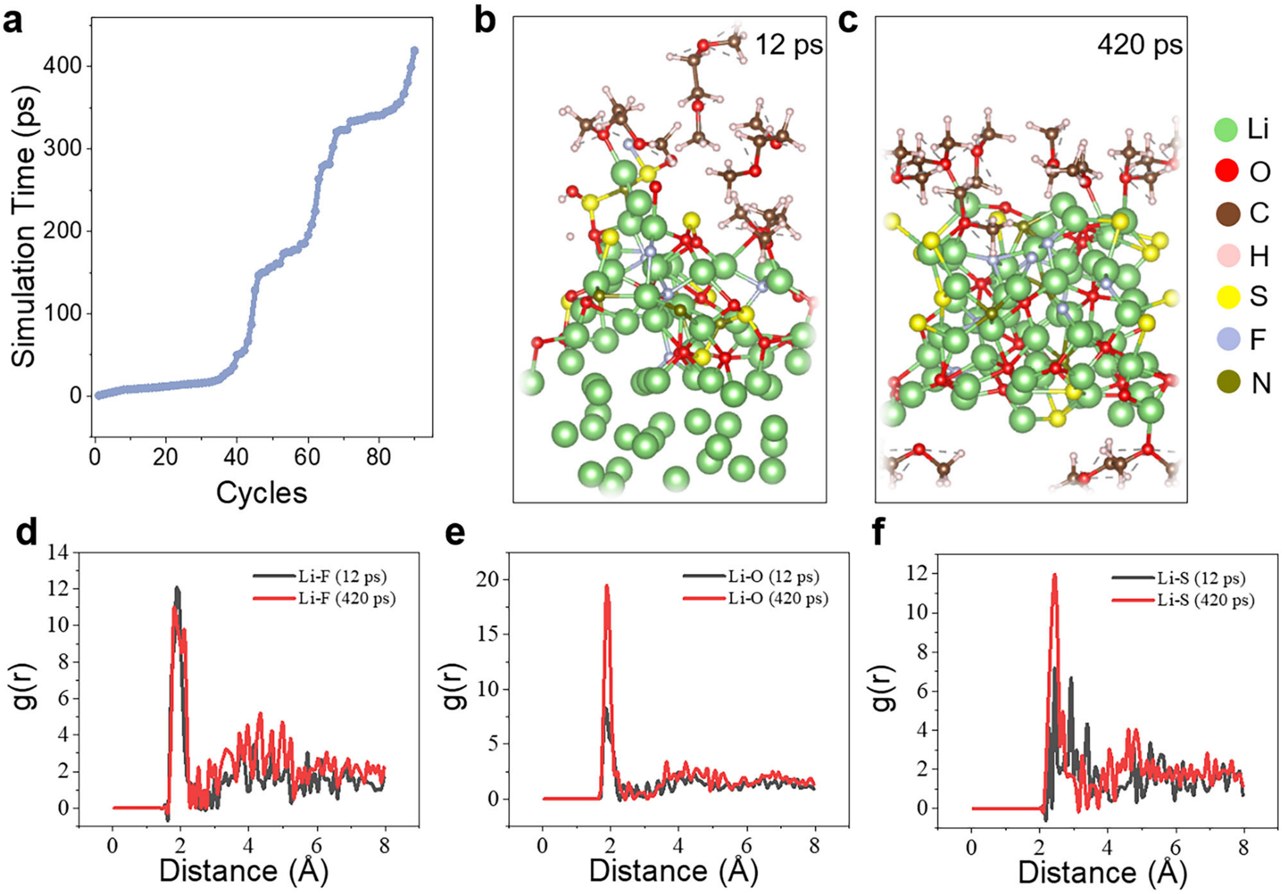

Fig. 3 | Demonstration of HAML for simulation of Li metal and LiFSI, DME mixed solution interface system. **a** The relationship between HAML cycles and simulation time. The snapshots of HAML simulations for Li metal and LiFSI, DME mixed solution interface system after 12 ps (**b**) and after 420 ps (**c**). The comparison of radial distribution functions for Li–F (**d**), Li–O (**e**), and Li–S (**f**) after 12 ps and 420 ps.

Fig. 4 | HAML simulation of the interface between Li metal and Li_6PS_5Cl system. **a** The relationship between HAML cycles and simulation time. **b–d** The snapshots during the simulation process. **e** The comparison of bond numbers for P–S, Li–P, Li–S, and Li–Cl bonds at initial time and after 528 ps. **f** The comparison of radial distribution functions for P–S at initial time and after 528 ps.

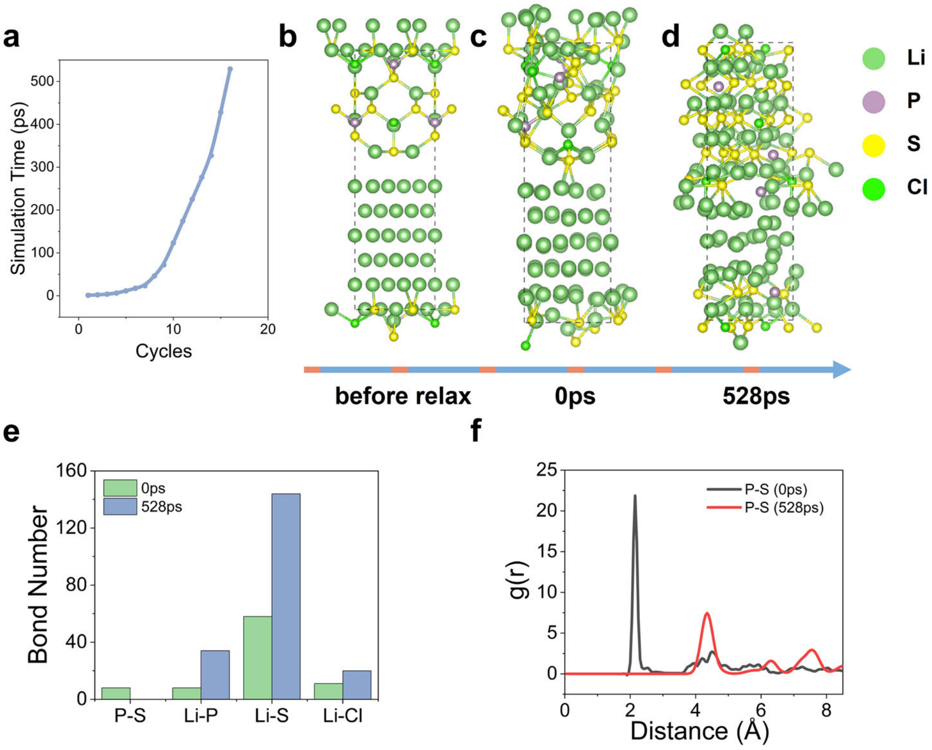

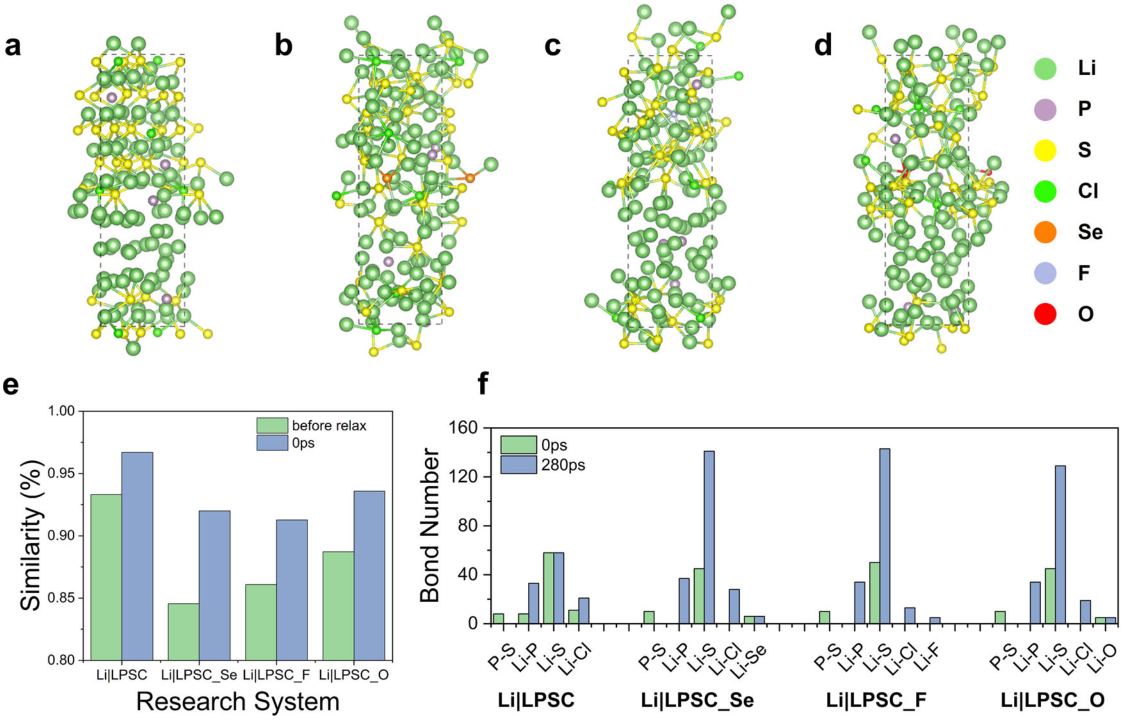

Fig. 5 | Comparison of interface reactions in four researched systems (Li|LPSC, Li|LPSC_Se, Li|LPSC_F, and Li|LPSC_O). Atomic configurations of Li|LPSC (**a**), Li|LPSC_Se (**b**), Li|LPSC_F (**c**), and Li|LPSC_O (**d**) interfaces after 280 ps HAML simulations. **e** The quantitative comparison of interface structure similarities between initial (interfaces before relaxation and AIMD simulation) and post-simulation interface configurations (after 280 ps). **f** The variations in bond numbers at the interfaces during the 280 ps HAML simulations.

has been found to improve interface stability and ionic conductivity in LPSC SSEs[9,10], while F[60] and O[61] are also recognized as beneficial doping elements for protecting the interface. Thus, we used the HAML method to systematically study the interfaces between Li metal and three element-doped LPSC electrolytes. The HAML simulation process for these doped systems, including detailed structural evolution and corresponding RDFs, is illustrated in Supplementary Figs. 11–13.

The pristine LPSC remains partially unreacted after 280 ps of simulations (Fig. 5a), while its doped variants, LPSC_Se, LPSC_F, and LPSC_O, exhibit enhanced interface reactivity at room temperature (Fig. 5b–d). This difference in reactivity is quantitatively corroborated by similarity analysis in Fig. 5e. The LPSC demonstrates the highest structural fidelity (>93%) among all systems, indicating that the LPSC interface structure remains relatively stable in the HAML simulation. This stability aligns with previous discussions. In contrast, the doped interfaces undergo significant structural evolutions throughout the simulation. The structural variations during HAML simulation reveal that dopant incorporation (Se, F, O) introduces structural perturbations that destabilize the native equilibrium configuration, which further promote progressive electrolyte decompositions. This inherent instability in the interface structure contributes to rapid reaction kinetics during the early stages of SEI formation at the interfaces of Li metal and LPSC_Se, LPSC_F, and LPSC_O. Despite the disappearance of P–S bonds across all LPSC interfaces indicating the breakdown of the PS_4^{2-} polyhedron, the doped interface structures exhibit significant variations in bonding configurations. As shown in Fig. 5f, the doped systems (LPSC_Se, LPSC_F, and LPSC_O) exhibit a more pronounced increase in Li–S, Li–P, and Li–Cl bond formations compared to the pristine LPSC after 280 ps of HAML simulation. Additionally, the F-doped interface forms stable Li–F bonds, contributing to the formation of a robust SEI. Besides, we analyzed the time-dependent evolution of bond formation to compare interfacial kinetics between doped and undoped systems. As shown in Supplementary Figs. 14 and 15, dopants accelerate interfacial reactions, leading to faster bond-breaking and associated processes.

During the HAML simulation of Li|LPSC_Se interface for 566 ps at 300 K (Supplementary Fig. 11a), the Li atoms in Li layers were found actively diffused into $Li_6PS_{4.75}Se_{0.25}Cl$ layer and reacted obviously, forming Li_2S, LiCl, Li_3P, and Li_4Se (Supplementary Fig. 11b–d), which is further demonstrated by the radial distribution functions in Supplementary Fig. 11e–h. The reactivity is more obvious compared to Li_6PS_5Cl|Li, and is similar to previous AIMD simulations, indicating that the dopant Se accelerated the reaction kinetics and helped to form ordered SEI[62]. In detail, Se promoted the diffusion of P and Cl into Li layers and the formation of relatively stable SEI containing more Li_3P than in Li|LPSC. The rapid degradation of PS_4^{2-} polyhedron, diffusion of P atoms into Li layers, and formation of Li_3P was also observed in F-doped and O-doped interfaces (Supplementary Figs. 12 and 13). These metastable doped configurations facilitate rapid interface reaction kinetics during the initial cycling stages. However, reactivity at the early stages of SEI formation may benefit the overall interfacial stability. The Se-doped, F-doped, and O-doped LPSC lead to the establishment of passive SEI as protection layers at the SSE|Li interface and ensure better electrochemical performance[60,61,63].

In addition to the metastable doped structures, the unstable crystal facets at the interface region also facilitate the formation of a relatively stable protective layer. An AIMD study by Golov et al. revealed distinct coordination environments across different crystallographic orientations[58]. The Li(110)|LPSC(110) and Li(111)|LPSC(111) interfaces exhibit higher interfacial degradation rates compared to Li(100)|LPSC(100) and Li(221)|LPSC(100) models. Specifically, the LPSC(111) facet exhibits higher surface energy than other orientations[64], and this observed variation in degradation behavior implies that interfacial degradation rates correlate with surface stability anisotropy. Furthermore, the Li(111)|LPSC(111) interface exhibits a reduced Li-ion migration barrier, facilitating enhanced ionic diffusion across the interface and thereby lowering interfacial resistance. Interestingly, despite LPSC's thermodynamic instability under standard conditions, experimental studies have successfully used it as a protective interlayer between high-entropy $Li_{2.75}Y_{0.16}Er_{0.16}Yb_{0.16}In_{0.25}Zr_{0.25}Cl_6$ and Li-In anodes[65]. This implementation indicates that reactivity at the LPSC|Li-In interface could contribute to stable solid-electrolyte interphase (SEI) formation, ultimately enhancing lithium battery cycling performance.

Discussion

In summary, this work presents a novel approach that combines AIMD with MLP, enabling accurate and efficient modeling of electrode-electrolyte interfaces. By applying HAML to representative systems involving both liquid and solid-state electrolytes reacting with Li metal, we demonstrated its advantages in both accuracy and computational efficiency. HAML effectively addresses key challenges in interface modeling and enables stable long-timescale simulation of interface reactions. For exploring interface reactions, an accurate MD simulation is typically sufficient to capture the reaction process and products, while AL may introduce unnecessary complexity. AL strategies still face challenges in exploring unknown reaction configurations and often lead to excessive computational costs. In contrast, HAML is an in situ approach, leveraging AIMD simulations to guide the reaction pathway accurately. This approach eliminates redundant configuration space exploration, allowing researchers to concentrate on key scientific questions within a single simulation. We believe the key advancement of HAML lies in its ability to achieve the desired outcome, regardless of the complexity of the interface reactions, with relatively low cost and effort. This is especially crucial for future high-throughput screening of electrolyte systems or doping elements that enhance interface stability, an area often neglected in previous work due to its high cost. High-throughput screening often involves multiple elements and systems, making it extremely complex and time-consuming when relying on traditional methods. Thus, HAML is well-positioned as a comprehensive framework for efficiently predicting interface evolution across diverse scenarios, playing a crucial role in optimizing interface properties and enhancing overall battery performance in practical applications.

Moreover, we employed HAML to gain deeper insights into the complex mechanisms governing interface reactions in Li metal anode. For liquid electrolytes, HAML accurately captured the dynamic evolution of SEI components with high temporal and spatial resolution. For solid-state electrolytes, HAML revealed the formation and stabilization of interphase layers, providing insights into their compatibility with Li metal. Specifically, for the chloride solid-state electrolyte LPSC, we introduced dopants such as Se, F, and O to modify the interfacial structure and reactivity between the electrolyte and Li metal anode. The intrinsic instability of the doped LPSC structure accelerates interface reaction kinetics and promotes the formation of the interface protection layer, thereby improving the overall stability of the full-cell system. In conjunction with previous studies[58,64], unstable crystal facets at the interface can facilitate the formation of a more stable protective layer, with degradation behavior varying across different crystallographic orientations due to surface stability anisotropy. Thus, introducing moderate lattice instability could serve as an effective strategy for modulating interface reaction kinetics, generating the stable SEI layer, and mitigating further degradation. These findings not only deepen our understanding of interface processes but also pave the way for the rational design of strategies to enhance the stability and performance of next-generation energy storage systems.

Despite the promising capabilities of HAML, several considerations are crucial for ensuring its reliable application. Among these, careful selection of key parameters, such as the maximum level lev_{max} and the break threshold γ_{break} of MTP, is essential for ensuring the accuracy and robustness of HAML. Proper tuning of these parameters is essential before applying HAML in practice. In particular, the break threshold may need to be set as small as possible for certain systems to maintain simulation accuracy. In this work, we primarily used the MTP as an example to demonstrate the effectiveness of the HAML framework. It is acknowledged that HAML still has certain limitations. In future research, HAML could be further refined and expanded for broader applications. By coupling alternative potential models, with magnetic or charge information, into the framework while retaining the uncertainty-based thresholding scheme, the performance and applicability of HAML could be further enhanced. Another promising direction is integrating HAML with universal large atomic models, potentially enhancing the transferability among a wide range of systems and eliminating the need for extensive MLP training. This advancement would significantly enhance the efficiency and adaptability of HAML, enabling its rapid application to novel chemistries or interfaces. As for potential applications, HAML simulations can be leveraged for high-throughput screening to identify materials or doping elements from extensive candidate databases that could enhance interface properties.

Methods

AIMD

The core of HAML lies in the iterative cycles between AIMD, MLP training, and MLP-MD. All the AIMD simulations were performed by the Vienna ab initio simulation package (VASP)[66,67]. The generalized gradient approximation (GGA) with a parametrized exchange-correlation function according to Perdew, Burke, and Ernzerhof (PBE) was used in the calculations[68]. The valence electron wave functions were expanded in the plane wave basis sets, and the projector augmented wave (PAW) method was used to describe the core-electron interactions[69]. The Grimme's D3 method was used to account for dispersion effects[70]. The energy cutoff for these simulations was 520 eV, and a 1 × 1 × 1 k-point mesh was used. The NVT ensemble was used in all the simulations, and the Nose–Hoover[71] thermostat was applied for temperature control. A timestep of 1 fs was used in all AIMD simulations.

MLP

We adopted the MTP[44,45] as the MLP module in the HAML framework. The rotationally covariant tensors are as follows,

$$M_{\mu,\nu}(n_i) = \sum_j f_\mu(|r_{ij}|, z_i, z_j)\,\underbrace{r_{ij}\otimes\cdots\otimes r_{ij}}_{\nu\ \text{times}}$$

where $f_\mu(|r_{ij}|, z_i, z_j)$ is the radial function

$$f_\mu\left(|r_{ij}|, z_i, z_j\right) = \sum_k c^{(k)}_{\mu,z_i,z_j} T_{(k)}(|r_{ij}|)(|r_{ij}| - r_c)^2$$

$T_{(k)}(|r_{ij}|)$ are the Chebyshev polynomials, k is the degree of polynomial, $c^{(k)}_{\mu,z_i,z_j}$ is the radial coefficients, and r_c is the cutoff radius. $r_{ij}\otimes\cdots\otimes r_{ij}$ is a tensor of rank ν encoding angular information.

The basis functions $B_\alpha(n_i)$ are formulated by contracting the moment tensors $M_{\mu,\nu}$ to a scalar. The linear regression model is built for the contracted basis functions $B_\alpha(n_i)$ and the atomic energy $V(n_i)$:

$$V\left(n_i\right) = \sum_\alpha C_\alpha B_\alpha(n_i)$$

where C_α is the linear coefficient.

For MLP training, parameters $lev_{\max}$ was set as 12, and the r_c was chosen to be 5.0 in all cases. These settings are designed to balance accuracy and efficiency. For MLP-MD simulations, the break threshold γ_{break} was selected as 10 and 20 in the systems of Li metal and solid-state electrolytes as well as Li metal and liquid electrolytes, respectively. All the MLP-MD simulations were conducted using the large-scale atomic/molecular massively parallel simulator (LAMMPS)[72]. The NVT ensemble was used in all the simulations, and the temperature was controlled using the Nose–Hoover algorisms[71]. A timestep of 0.5 fs was used in all MLP-MD simulations. All the configurations were visualized using the VESTA software[73].

Data availability

The authors declare that all data supporting the findings of this study are available from the corresponding author upon reasonable request.

Received: 21 April 2025; Accepted: 19 July 2025;

References

1. Seh, Z. W. et al. Combining theory and experiment in electrocatalysis: Insights into materials design. *Science* **355**, eaad4998 (2017).
2. Salanne, M. et al. Efficient storage mechanisms for building better supercapacitors. *Nat. Energy* **1**, 1–10 (2016).
3. Scalfi, L., Salanne, M. & Rotenberg, B. Molecular simulation of electrode-solution interfaces. *Annu. Rev. Phys. Chem.* **72**, 189–212 (2021).
4. Tarascon, J.-M. & Armand, M. Issues and challenges facing rechargeable lithium batteries. *Nature* **414**, 359–367 (2001).
5. Albertus, P., Babinec, S., Litzelman, S. & Newman, A. Status and challenges in enabling the lithium metal electrode for high-energy and low-cost rechargeable batteries. *Nat. Energy* **3**, 16–21 (2018).
6. Liu, J. et al. Pathways for practical high-energy long-cycling lithium metal batteries. *Nat. Energy* **4**, 180–186 (2019).
7. Liu, B., Zhang, J.-G. & Xu, W. Advancing lithium metal batteries. *Joule* **2**, 833–845 (2018).
8. Qian, J. et al. High rate and stable cycling of lithium metal anode. *Nat. Commun.* **6**, 6362 (2015).
9. Epp, V., Gün, Ö, Deiseroth, H.-J. & Wilkening, M. Highly mobile ions: low-temperature NMR directly probes extremely fast Li^+ hopping in argyrodite-type Li_6PS_5. *Br. J. Phys. Chem. Lett.* **4**, 2118–2123 (2013).
10. Chen, H. M., Maohua, C. & Adams, S. Stability and ionic mobility in argyrodite-related lithium-ion solid electrolytes. *Phys. Chem. Chem. Phys.* **17**, 16494–16506 (2015).
11. Xu, Y. et al. Promoting mechanistic understanding of lithium deposition and solid-electrolyte interphase (SEI) formation using advanced characterization and simulation methods: recent progress, limitations, and future perspectives. *Adv. Energy Mater.* **12**, 2200398 (2022).
12. Wagner-Henke, J. et al. Knowledge-driven design of solid-electrolyte interphases on lithium metal via multiscale modelling. *Nat. Commun.* **14**, 6823 (2023).
13. Yao, N., Chen, X., Fu, Z.-H. & Zhang, Q. Applying classical, ab initio, and machine-learning molecular dynamics simulations to the liquid electrolyte for rechargeable batteries. *Chem. Rev.* **122**, 10970–11021 (2022).
14. Qi, J., Ko, T. W., Wood, B. C., Pham, T. A. & Ong, S. P. Robust training of machine learning interatomic potentials with dimensionality reduction and stratified sampling. *npj Comput. Mater.* **10**, 43 (2024).
15. Young, J., Kulick, P. M., Juran, T. R. & Smeu, M. Comparative study of ethylene carbonate-based electrolyte decomposition at Li, Ca, and Al anode interfaces. *ACS Appl. Energy Mater.* **2**, 1676–1684 (2019).
16. Leung, K. Electronic structure modeling of electrochemical reactions at electrode/electrolyte interfaces in lithium ion batteries. *J. Phys. Chem. C***117**, 1539–1547 (2013).
17. Camacho-Forero, L. E., Smith, T. W. & Balbuena, P. B. Effects of high and low salt concentration in electrolytes at lithium–metal anode surfaces. *J. Phys. Chem. C***121**, 182–194 (2017).
18. Camacho-Forero, L. E. & Balbuena, P. B. Effects of charged interfaces on electrolyte decomposition at the lithium metal anode. *J. Power Sources* **472**, 228449 (2020).
19. Behler, J. Perspective. Machine learning potentials for atomistic simulations. *J. Chem. Phys.* **145**, 170901 (2016).
20. Mishin, Y. Machine-learning interatomic potentials for materials science. *Acta Mater.* **214**, 116980 (2021).
21. Zuo, Y. et al. Performance and cost assessment of machine learning interatomic potentials. *J. Phys. Chem. A* **124**, 731–745 (2020).
22. Liu, Y. et al. Data quantity governance for machine learning in materials science. *Natl. Sci. Rev.* **10**, nwad125 (2023).
23. Deringer, V. L., Caro, M. A. & Csányi, G. Machine learning interatomic potentials as emerging tools for materials science. *Adv. Mater.* **31**, 1902765 (2019).
24. Qi, J. et al. Machine learning moment tensor potential for modeling dislocation and fracture in L1 0-TiAl and D0 19-Ti 3 Al alloys. *Phys. Rev. Mater.* **7**, 103602 (2023).
25. Lai, G. et al. The mechanism of external pressure suppressing dendrites growth in Li metal batteries. *J. Energy Chem.* **79**, 489–494 (2023).
26. Lai, G. et al. The mechanism of Li deposition on the Cu substrates in the anode-free Li metal batteries. *Small* **19**, 2205416 (2023).
27. Lee, T. et al. Atomic-scale origin of the low grain-boundary resistance in perovskite solid electrolyte Li0. 375Sr0. 4375Ta0. 75Zr0. 25O3. *Nat. Commun.* **14**, 1940 (2023).
28. Qi, J. et al. Bridging the gap between simulated and experimental ionic conductivities in lithium superionic conductors. *Mater. Today Phys.* **21**, 100463 (2021).
29. Gong, S. et al. A predictive machine learning force-field framework for liquid electrolyte development. *Nature Machine Intelligence* **7**, 534–552 (2025).
30. Holekevi Chandrappa, M. L., Qi, J., Chen, C., Banerjee, S. & Ong, S. P. Thermodynamics and kinetics of the cathode–electrolyte interface in all-solid-state Li–S batteries. *J. Am. Chem. Soc.* **144**, 18009–18022 (2022).
31. Ko, T. W. & Ong, S. P. Recent advances and outstanding challenges for machine learning interatomic potentials. *Nat. Comput. Sci.* **3**, 998–1000 (2023).
32. Liu, Y. & Mo, Y. Learning from models: high-dimensional analyses on the performance of machine learning interatomic potentials. *npj Comput. Mater.* **10**, 159 (2024).
33. Sundararaman, R. & Schwarz, K. Evaluating continuum solvation models for the electrode-electrolyte interface: Challenges and strategies for improvement. *J. Chem. Phys.* **146**, 084111 (2017).
34. Vandermause, J. et al. On-the-fly active learning of interpretable Bayesian force fields for atomistic rare events. *npj Comput. Mater.* **6**, 20 (2020).
35. Kulichenko, M. et al. Uncertainty-driven dynamics for active learning of interatomic potentials. *Nat. Comput. Sci.* **3**, 230–239 (2023).
36. van der Oord, C., Sachs, M., Kovács, D. P., Ortner, C. & Csányi, G. Hyperactive learning for data-driven interatomic potentials. *npj Comput. Mater.* **9**, 168 (2023).
37. Yang, Y., Zhang, S., Ranasinghe, K. D., Isayev, O. & Roitberg, A. E. Machine learning of reactive potentials. *Annu. Rev. Phys. Chem.* **75**, 371–395 (2024).
38. Tharwat, A. & Schenck, W. A survey on active learning: State-of-the-art, practical challenges and research directions. *Mathematics* **11**, 820 (2023).
39. Friederich, P., Häse, F., Proppe, J. & Aspuru-Guzik, A. Machine-learned potentials for next-generation matter simulations. *Nat. Mater.* **20**, 750–761 (2021).
40. Fu, X. et al. Forces are not enough: Benchmark and critical evaluation for machine learning force fields with molecular simulations. Preprint at https://arxiv.org/abs/2210.07237 (2022).
41. Cui, T. et al. Online test-time adaptation for better generalization of interatomic potentials to out-of-distribution data. *Nat. Commun.* **16**, 1891 (2025).
42. Xu, L., Shao, W., Jin, H. & Wang, Q. Data Efficient and stability indicated sampling for developing reactive machine learning potential to achieve ultralong simulation in lithium-metal batteries. *J. Phys. Chem. C***127**, 24106–24117 (2023).
43. Liu, Y. et al. Effects of high and low salt concentrations in electrolytes at lithium–metal anode surfaces using DFT-ReaxFF hybrid molecular dynamics method. *J. Phys. Chem. Lett.* **12**, 2922–2929 (2021).
44. Shapeev, A. V. Moment tensor potentials: a class of systematically improvable interatomic potentials. *Multiscale Model. Simul.* **14**, 1153–1173 (2016).
45. Novikov, I. S., Gubaev, K., Podryabinkin, E. V. & Shapeev, A. V. The MLIP package: moment tensor potentials with MPI and active learning. *Mach. Learn. Sci. Technol.* **2**, 025002 (2020).
46. Wan, C. et al. Multinuclear NMR study of the solid electrolyte interface formed in lithium metal batteries. *ACS Appl. Mater. Interfaces* **9**, 14741–14748 (2017).

47. Chen, Y. et al. Origin of dendrite-free lithium deposition in concentrated electrolytes. *Nat. Commun.* **14**, 2655 (2023).
48. Zhang, H., Shen, C., Huang, Y. & Liu, Z. Spontaneously formation of SEI layers on lithium metal from LiFSI/DME and LiTFSI/DME electrolytes. *Appl. Surf. Sci.* **537**, 147983 (2021).
49. Deiseroth, H. J. et al. Li_6PS_5X: a class of crystalline Li-rich solids with an unusually high Li^+ mobility. *Angew. Chem. Int. Ed.* **47**, 755–758 (2008).
50. Rao, R. P. & Adams, S. Studies of lithium argyrodite solid electrolytes for all-solid-state batteries. *Phys. Status Solidi A* **208**, 1804–1807 (2011).
51. Deng, Z., Zhu, Z., Chu, I.-H. & Ong, S. P. Data-driven first-principles methods for the study and design of alkali superionic conductors. *Chem. Mater.* **29**, 281–288 (2016).
52. Holekevi Chandrappa, M. L., Qi, J., Chen, C., Banerjee, S. & Ong, S. P. Thermodynamics and kinetics of the cathode-electrolyte interface in all-solid-state Li-S batteries. *J. Am. Chem. Soc.* **144**, 18009–18022 (2022).
53. Jalem, R., Chandrappa, M. L. H., Qi, J., Tateyama, Y. & Ong, S. P. Lithium dynamics at grain boundaries of β-Li_3PS_4 solid electrolyte. *Energy Adv.* **2**, 2029–2041 (2023).
54. Richards, W. D., Miara, L. J., Wang, Y., Kim, J. C. & Ceder, G. Interface stability in solid-state batteries. *Chem. Mater.* **28**, 266–273 (2015).
55. Cheng, T., Merinov, B. V., Morozov, S. & Goddard, W. A. Quantum mechanics reactive dynamics study of solid Li-electrode/Li_6PS_5Cl-electrolyte interface. *ACS Energy Lett.* **2**, 1454–1459 (2017).
56. Yu, C. et al. Unravelling Li-ion transport from picoseconds to seconds: bulk versus interfaces in an argyrodite Li_6PS_5Cl-Li_2S all-solid-state Li-Ion battery. *J. Am. Chem. Soc.* **138**, 11192–11201 (2016).
57. Wenzel, S., Sedlmaier, S. J., Dietrich, C., Zeier, W. G. & Janek, J. Interfacial reactivity and interphase growth of argyrodite solid electrolytes at lithium metal electrodes. *Solid State Ion.* **318**, 102–112 (2018).
58. Golov, A. & Carrasco, J. Molecular-level insight into the interfacial reactivity and ionic conductivity of a Li-argyrodite Li_6PS_5Cl solid electrolyte at bare and coated Li-metal anodes. *ACS Appl. Mater. Interfaces* **13**, 43734–43745 (2021).
59. Chaney, G., Golov, A., van Roekeghem, A., Carrasco, J. & Mingo, N. Two-step growth mechanism of the solid electrolyte interphase in argyrodyte/Li-metal contacts. *ACS Appl. Mater. Interfaces* **16**, 24624–24630 (2024).
60. Arnold, W. et al. Synthesis of fluorine-doped lithium argyrodite solid electrolytes for solid-state lithium metal batteries. *ACS Appl. Mater. Interfaces* **14**, 11483–11492 (2022).
61. Wu, M., Liu, G. & Yao, X. Oxygen doped argyrodite electrolyte for all-solid-state lithium batteries. *Appl. Phys. Lett.* **121**, 203904 (2022).
62. Golov, A. & Carrasco, J. Unveiling solid electrolyte interphase formation at the molecular level: computational insights into bare Li-metal anode and $Li_6PS_{5-x}Se_xCl$ argyrodite solid electrolyte. *ACS Energy Lett.* **8**, 4129–4135 (2023).
63. Kim, H.-M., Subramanian, Y. & Ryu, K.-S. Improved electrochemical and air stability performance of SeS_2 doped argyrodite lithium superionic conductors for all-solid-state lithium batteries. *Electrochim. Acta* **442**, 141869 (2023).
64. Camacho-Forero, L. E. & Balbuena, P. B. Elucidating interfacial phenomena between solid-state electrolytes and the sulfur-cathode of lithium–sulfur batteries. *Chem. Mater.* **32**, 360–373 (2019).
65. Song, Z. et al. Promoting high-voltage stability through local lattice distortion of halide solid electrolytes. *Nat. Commun.* **15**, 1481 (2024).
66. Kresse, G. & Furthmüller, J. Efficient iterative schemes for ab initio total-energy calculations using a plane-wave basis set. *Phys. Rev. B* **54**, 11169–11186 (1996).
67. Kresse, G. & Furthmüller, J. Efficiency of ab-initio total energy calculations for metals and semiconductors using a plane-wave basis set. *Comput. Mater. Sci.* **6**, 15–50 (1996).
68. Perdew, J. P., Burke, K. & Ernzerhof, M. Generalized gradient approximation made simple. *Phys. Rev. Lett.* **77**, 3865–3868 (1996).
69. Blöchl, P. E. Projector augmented-wave method. *Phys. Rev. B* **50**, 17953–17979 (1994).
70. Grimme, S., Antony, J., Ehrlich, S. & Krieg, H. A consistent and accurate ab initio parametrization of density functional dispersion correction (DFT-D) for the 94 elements H-Pu. *J. Chem. Phys.* **132**, 154104 (2010).
71. Martyna, G. J., Klein, M. L. & Tuckerman, M. Nosé–Hoover chains: the canonical ensemble via continuous dynamics. *J. Chem. Phys.* **97**, 2635–2643 (1992).
72. Plimpton, S. Fast parallel algorithms for short-range molecular dynamics. *J. Comput. Phys.* **117**, 1–19 (1995).
73. Momma, K. & Izumi, F. VESTA 3 for three-dimensional visualization of crystal, volumetric and morphology data. *J. Appl. Crystallogr.* **44**, 1272–1276 (2011).

Acknowledgements

This work was supported by the National Natural Science Foundation of China (No. 12426301), Shenzhen Science and Technology Research Grant (No. 20231117083459001), and AI for Science (AI4S)-Preferred Program, Peking University, Shenzhen, China.

Author contributions

G.L. and R.Z. contributed equally to this work. J. Zheng and Y. Z. supervised the project. G.L. conceived the idea and designed the HAML method. G.L. and R.Z. performed the HAML simulations. G.L., R.Z., C.F., J. Zhao, T.C., and Y.Z. analyzed the data and interpreted the results. J. Zheng, Y.Z., and B.X. offered insight and guidance throughout the project. G.L. and R.Z. wrote the manuscript. J. Zheng and Y.Z. revised the manuscript. All authors contributed to the scientific discussion and approved the manuscript.

Competing interests

The authors declare no competing interests.

Additional information

Supplementary information The online version contains supplementary material available at https://doi.org/10.1038/s41524-025-01747-7.

Correspondence and requests for materials should be addressed to Yunxing Zuo, Bo Xu or Jiaxin Zheng.

Reprints and permissions information is available at http://www.nature.com/reprints